Front. Phys. 10(6), 102501 (2015)
DOI 10.1007/s11467-015-0479-8

REVIEW ARTICLE

Dynamical effects of spin-dependent interactions in low- and intermediate-energy heavy-ion reactions

Jun Xu[1,2,†], **Bao-An Li**[3], **Wen-Qing Shen**[1], **Yin Xia**[1,4]

[1] *Shanghai Institute of Applied Physics, Chinese Academy of Sciences, Shanghai 201800, China*
[2] *Kavli Institute for Theoretical Physics China, Chinese Academy of Sciences, Beijing 100190, China*
[3] *Department of Physics and Astronomy, Texas A&M University–Commerce, Commerce, TX 75429-3011, USA*
[4] *University of Chinese Academy of Sciences, Beijing 100049, China*

Corresponding author. E-mail: [†]*xujun@sinap.ac.cn*

Received June 19, 2015; accepted July 29, 2015

It is well known that noncentral nuclear forces, such as the spin–orbital coupling and the tensor force, play important roles in understanding many interesting features of nuclear structures. However, their dynamical effects in nuclear reactions are poorly known because only the spin-averaged observables are normally studied both experimentally and theoretically. Realizing that spin-sensitive observables in nuclear reactions may convey useful information about the in-medium properties of noncentral nuclear interactions, besides earlier studies using the time-dependent Hartree–Fock approach to understand the effects of spin–orbital coupling on the threshold energy and spin polarization in fusion reactions, some efforts have been made recently to explore the dynamical effects of noncentral nuclear forces in intermediate-energy heavy-ion collisions using transport models. The focus of these studies has been on investigating signatures of the density and isospin dependence of the form factor in the spin-dependent single-nucleon potential. Interestingly, some useful probes were identified in the model studies but so far there are still no data to compare with. In this brief review, we summarize the main physics motivations as well as the recent progress in understanding the spin dynamics and identifying spin-sensitive observables in heavy-ion reactions at intermediate energies. We hope the interesting, important, and new physics potentials identified in the spin dynamics of heavy-ion collisions will stimulate more experimental work in this direction.

Keywords heavy-ion collisions, transport model, spin–orbit interaction, tensor force, polarization

PACS numbers 25.70.-z, 21.30.Fe, 21.10.Hw

Contents

1 Introduction

Understanding novel features of the fundamental nuclear forces and properties of strongly interacting matter under extreme conditions of density, temperature, spin, and isospin is among the main goals of nuclear physics. Heavy-ion collision (HIC) experiments play an important role in achieving these goals. Indeed, great achievements have been made using HICs at various beam energies from the sub-Colomb barrier to the highest energy available at the Large Hadron Collider. In particular, terrestrial experiments using intermediate-energy HICs have led to strong constraints on the equations of state of hadronic matter [1] and neutron-rich nucleonic matter [2, 3].

*Special Topic: Spin Physics (Eds. Haiyan Gao & Bo-Qiang Ma).

Theoretical studies have shown recently that some spin-sensitive observables of HICs can be used to explore the in-medium properties of noncentral nuclear forces. The spin-dependent nuclear interactions are important for explaining several interesting features of nuclear structure [4], such as the varying magic numbers and the shell evolution with the isospin asymmetry of finite nuclei. However, the strength, density, and isospin dependence of the nuclear spin–orbit coupling are still uncertain (see Section 2.1). Moreover, the tensor force can modify the magic number of nuclei and is an important source of the nucleon–nucleon short-range correlation. The latter is related to many interesting phenomena in nuclear physics (see Section 2.2). More studies on in-medium properties of the spin–orbit coupling and tensor force are thus very much needed. HICs provide flexible ways of adjusting the conditions of the nuclear medium and may also lead to new spin-dependent phenomena. For example, the so-called spin Hall effect [5–7], which affects the dynamics of spin-up and spin-down particles differently as a result of the spin–orbit coupling, is expected to be a general feature in any spin transport process. It thus might be interesting to test whether such a phenomenon can also occur in HICs.

Considerable efforts using the time-dependent Hartree–Fock (TDHF) model, the spin- and isospin-dependent Boltzmann–Uehling–Uhlenbeck (SIBUU) transport model, and the quantum molecular dynamics (QMD) model have been devoted to exploring the spin dynamics in HICs (see Section 3). Indeed, some interesting phenomena were found. For example, it was found that the inclusion of the spin-dependent nuclear interaction may affect the fusion threshold, generate the spin twist during the collision process, and lead to the spin splitting of nucleon collective flows (see Section 3). Future comparisons with relevant experimental data may help extract properties of the in-medium spin-dependent nuclear force. Here we review briefly the main physics motivations and recent findings of studying the spin-dependent dynamics and observables in low- and intermediate-energy HICs. A major goal of this article is to stimulate more experimental work in this direction.

2 Spin-related nuclear force

Based on the one-boson-exchange picture [8], the nuclear force can be understood by exchanging mesons between nucleons. Exchanging the scalar σ meson and vector ω meson leads to, respectively, attractive and repulsive central nuclear forces as well as the spin–orbit interaction, while exchanging the π meson and ρ meson leads to, respectively, long-range and short-range nuclear tensor forces. Although in free space the bare nuclear force is well constrained by the nucleon–nucleon scattering data, the in-medium nuclear interactions, especially the nuclear spin–orbit interaction and tensor force, are still quite uncertain. The in-medium nuclear interactions can be studied by using microscopic many-body theories or phenomenological models, such as the nonrelativistic Skyrme–Hartree–Fock (SHF) model and the relativistic mean-field (RMF) model. In the following subsections, we will discuss the effective spin-dependent nuclear force based on the energy-density functional in the phenomenological approach.

2.1 Nuclear spin–orbit interaction

The nuclear spin–orbit interaction was first introduced to explain the magic numbers of nuclei [9, 10]. Nuclei with numbers of neutrons or protons equal to the magic numbers are more stable, and this reflects the special shell structure of a nucleus. Although even a simple harmonic potential leads to the shell structure of nucleon energy levels inside nuclei, the spin–orbit coupling is essential to reproduce the correct magic number.

In the Skyrme interaction, the effective spin–orbit force between two nucleons at positions $\boldsymbol{r}_1$ and $\boldsymbol{r}_2$ can be expressed as [11]

$$V_{so} = \mathrm{i}W_0(\boldsymbol{\sigma}_1 + \boldsymbol{\sigma}_2) \cdot \boldsymbol{k} \times \delta(\boldsymbol{r}_1 - \boldsymbol{r}_2)\boldsymbol{k}', \tag{1}$$

where W_0 is the spin–orbit coupling constant, $\boldsymbol{\sigma}_1$ and $\boldsymbol{\sigma}_2$ are the Pauli matrices for the two nucleons, $\boldsymbol{k} = -\mathrm{i}(\nabla_1 - \nabla_2)/2$ is the relative momentum operator acting on the right side with ∇_1 and ∇_2 acting on the first and second nucleon, respectively, and $\boldsymbol{k}'$ is its complex conjugate acting on the left. From the conventional Hartree-Fock method, the spin–orbit single-particle potential can be obtained based on the above effective spin–orbit force as

$$U_q^{so} = \boldsymbol{W}_q \cdot (-\mathrm{i}\nabla \times \boldsymbol{\sigma}), \tag{2}$$

where

$$\boldsymbol{W}_q = \frac{W_0}{2}(\nabla\rho + \nabla\rho_q) \tag{3}$$

is the form factor of the spin–orbit potential, with $q = \mathrm{n}$ or p being the isospin index and ρ being the nucleon number density. By taking the operator $-\mathrm{i}\nabla$ as the momentum $\boldsymbol{p}$, the right-hand side of Eq. (2) has the form of $(\boldsymbol{r} \times \boldsymbol{p}) \cdot \boldsymbol{\sigma}$ with $\boldsymbol{W}_q$ playing the role of $\boldsymbol{r}$, and this is why it is called the spin–orbit potential. By solving the Schrödinger equation with the single-nucleon Hamiltonian

$$h_q = -\nabla \cdot \left(\frac{1}{2m_q^\star}\nabla\right) + U_q + U_q^{so}, \tag{4}$$

with $m_q^\star$ being the effective nucleon mass and U_q being the spin-independent potential, the single-nucleon spectrum in a spherical closed-shell nucleus can be obtained.

In the RMF model, one solves the Dirac equation, where the spin of the nucleon is treated explicitly with nucleon wave functions for different spin states [12]. Studies of SHF and RMF models on nuclear structure were reviewed in Ref. [13], and here we compare the effective spin–orbit potentials from both the relativistic and nonrelativistic approaches. With nonrelativistic expansion of the Dirac equation, the form factor of the nucleon effective spin–orbit potential in the RMF model can be expressed in the form [14, 15]

$$\boldsymbol{W}_{\rm RMF} = \frac{1}{(2m - C_{eff}\rho)^2} C_{eff}\nabla\rho, \tag{5}$$

where m is the nucleon mass and the coefficient C_{eff} is related to the coupling strength and mass of the scalar σ meson and the vector ω meson, i.e.,

$$C_{eff} = \frac{g_\sigma^2}{m_\sigma^2} + \frac{g_\omega^2}{m_\omega^2}. \tag{6}$$

The form factors of the spin–orbit potential in the SHF model [Eq. (3)] and the RMF model [Eq. (5)] are different. First, the spin–orbit coupling strength is a constant in the SHF model, but the effective coupling strength depends on the density in the RMF model. Implementing an additional density-dependent effective nucleon–nucleon spin–orbit interaction with a coupling constant W_1, the authors of Ref. [16] got additional contributions to the form factor as

$$\begin{aligned}\boldsymbol{W}_q^\rho = {} & \frac{W_1}{2}[c\rho\nabla(\rho-\rho_q) + (2+c)(2\rho_q)^c\nabla\rho_q] \\ & + \frac{W_1}{4}c\rho^{c-1}(\rho-\rho_q)\nabla\rho,\end{aligned} \tag{7}$$

with c mimicking the density dependence. The above form was tested in Ref. [16] in semi-infinite nuclear matter with parameters fitted to the RMF interaction. It was found that the general features of the RMF model were then reproduced with this nonrelativistic density-dependent spin–orbit interaction. Nevertheless, the density dependence of the spin–orbit coupling is still largely unknown so far, and it is related to many interesting phenomena in nuclear structure studies [17–19]. Second, the spin–orbit couplings from the SHF and RMF approaches have different isospin dependence; i.e., in the SHF approach the spin–orbit coupling is stronger for nucleons of the same isospin, whereas in the RMF approach the coupling strength is the same for neutrons and protons. This feature impacts descriptions of properties of neutron-rich nuclei, e.g., the kink in the evolution of the charge radii for lead isotopes. It was shown that the weak isospin dependence of the spin–orbit coupling in the RMF approach can better explain the kink than can the conventional SHF functional. However, if the form factor in the latter approach was modified to [20, 21]

$$\boldsymbol{W}_q = \frac{W_0}{2}(1+\chi_w)\nabla\rho_q + \frac{W_0}{2}\nabla\rho_{q'} \quad (q \neq q'), \tag{8}$$

a similar kink can be reproduced with $\chi_w \approx 0.1$ [21], corresponding to the case with a very small Fock contribution of the spin–orbit interaction. Similar efforts were made by using a modified SHF functional to reproduce the isospin dependence of the spin–orbit field in semi-infinite nuclear matter with different neutron excesses [22] and in neutron-rich nuclei [23] from a relativistic approach. In Ref. [24], the isospin dependence of the spin–orbit coupling was compared in light drip line nuclei from the RMF theory and the nonrelativistic Skyrme model. Furthermore, it was observed that the commonly used Skyrme functional of the spin–orbit splitting overestimated the central density and the spin–orbit splitting of neutron drops [25], calling for new functionals of the spin–orbit coupling. The proton energy splitting of $h_{11/2}$ and $g_{7/2}$ outside the $Z = 50$ closed shell increases with neutron excess, corresponding to the decreasing strength of the nuclear spin–orbit interaction [26]. The studies so far seem to favor a weak isospin dependence of the spin–orbit coupling. However, since the isospin dependence of the spin–orbit coupling, which is important in nuclear surfaces, is often coupled with its density dependence, it is still not well settled yet.

Based on the above discussion, we proposed the following general form of the form factor of the spin–orbit coupling by taking both the density and isospin dependence into account:

$$\boldsymbol{W}_q = \frac{W_0}{2}\left(\frac{\rho}{\rho_0}\right)^\gamma (a\nabla\rho_q + b\nabla\rho_{q'}) \quad (q \neq q'). \tag{9}$$

The above form is artificially constructed and, for simplicity, includes only the main physics. In the above form, γ is used to mimic the density dependence of the spin–orbit coupling while fixing its strength at saturation density ρ_0 to be W_0. a and b are parameters to vary the isospin dependence of the spin–orbit coupling, with $a = 2$ and $b = 1$ corresponding to the case of the standard SHF approach and $a = b$ corresponding to the case of the RMF approach. The values of γ, a, and b are still uncertain according to the above discussion. For the strength of the spin–orbit coupling W_0, efforts have been made to extract its information from ground-state properties

of various nuclei. Recent studies have shown that the spin–orbit coupling and the tensor force, which will be discussed in the next subsection, should be considered simultaneously to describe the spin–orbit splitting and single-nucleon spectra of nuclei. Based on the Skyrme functional and by taking the uncertainties of the tensor force into account, the strength of the spin–orbit coupling is ≈80–150 MeV fm^5, from fitting the properties of light to heavy nuclei [27–29].

The single-nucleon Hamlitonian of Eq. (4) is adequate to describe the ground-state properties of spherical closed-shell nuclei. For open-shell nuclei, one needs to consider an additional spin-dependent potential using the spin-current density $\boldsymbol{J}$ from Eq. (1):

$$U_q^J = -\frac{W_0}{2}\nabla\cdot(\boldsymbol{J}+\boldsymbol{J}_q). \tag{10}$$

$\boldsymbol{J}$ is actually the vector component of the spin-current density tensor $J_{\mu\nu}$ (see, e.g., Ref. [27] for a more detailed discussion). For deformed nuclei, not only the time-even potentials [Eqs. (2) and (10)] but also the time-odd potentials should be considered [30]. Starting from the effective nucleon–nucleon spin–orbit interaction [Eq. (1)] and taking Eq. (9) into consideration, one can obtain the general form of the time-even and time-odd spin-dependent potentials as

$$\begin{aligned} U_q^{s\text{-even}} &= -\frac{W_0}{2}\left(\frac{\rho}{\rho_0}\right)^\gamma[\nabla\cdot(a\boldsymbol{J}_q+b\boldsymbol{J}_{q'})] \\ &+\frac{W_0}{2}\left(\frac{\rho}{\rho_0}\right)^\gamma(a\nabla\rho_q+b\nabla\rho_{q'})\cdot(\boldsymbol{p}\times\boldsymbol{\sigma}), \end{aligned} \tag{11}$$

$$\begin{aligned} U_q^{s\text{-odd}} &= -\frac{W_0}{2}\left(\frac{\rho}{\rho_0}\right)^\gamma\boldsymbol{p}\cdot[\nabla\times(a\boldsymbol{s}_q+b\boldsymbol{s}_{q'})] \\ &-\frac{W_0}{2}\left(\frac{\rho}{\rho_0}\right)^\gamma\boldsymbol{\sigma}\cdot[\nabla\times(a\boldsymbol{j}_q+b\boldsymbol{j}_{q'})]\ (q\neq q'), \end{aligned} \tag{12}$$

where $\boldsymbol{p}=-\mathrm{i}\nabla$ is the momentum operator, and $\boldsymbol{s}$ and $\boldsymbol{j}$ are spin density and current density, respectively. We note that the time-odd potentials play an important role in the dynamics of heavy-ion reactions, which will be discussed in Section 3.

2.2 Nuclear tensor force

The first piece of strong evidence for the nuclear tensor force comes from studying properties of deuterons. In the nonrelativistic approach, the nuclear tensor force between two nucleons at positions $\boldsymbol{r}_1$ and $\boldsymbol{r}_2$ is often expressed with the tensor operator written as

$$S_{12}=3\frac{(\boldsymbol{\sigma}_1\cdot\boldsymbol{r})(\boldsymbol{\sigma}_2\cdot\boldsymbol{r})}{r^2}-(\boldsymbol{\sigma}_1\cdot\boldsymbol{\sigma}_2), \tag{13}$$

where $\boldsymbol{r}=\boldsymbol{r}_1-\boldsymbol{r}_2$ is the relative position vector. One thus sees that whether the tensor force is attractive or repulsive depends on the relative direction between the spin and the relative position vector; i.e., $S_{12}>0$ for $\boldsymbol{\sigma}_{1(2)}$ parallel to $\boldsymbol{r}$ and $S_{12}<0$ for $\boldsymbol{\sigma}_{1(2)}$ perpendicular to $\boldsymbol{r}$.

The tensor term in the effective nuclear interaction was first included in the Skyrme force [31], but afterward it was neglected owing to its complex form. Recently, it has attracted renewed interest. It has been found by Otsuka *et al.* that the nuclear tensor force may affect the shell structure or even modify the magic number of nuclei [32–34]. The combined effects of the spin–orbit coupling and the nuclear tensor force sometimes hamper our understanding of both of them [35, 36]. Based on the random phase approximation, the effects of the tensor force on the multipole response of magic nuclei have been studied, and a large effect on the magnetic dipole states was observed [37]. Moreover, it was proposed that the spin-isospin excitation of finite nuclei may serve as a useful observable to assess the strength of the tensor force [38, 39]. The existence of the tensor force may also open a shell gap for large neutron numbers, having a consequent implication for the synthesis of neutron-rich superheavy elements [40].

Although the nuclear tensor force has no effect on the equation of state of spin-saturated nuclear matter based on the studies at the mean-field level, it affects the properties of nuclear matter from many-body calculation beyond the mean field. It was found that the repulsive central force and the tensor force are two important sources of the nucleon–nucleon short-range correlation [41]. The high-momentum tail of the nucleon distribution in nuclear matter as well as in finite nuclei was observed even at zero temperature based on these studies [42–45]. Great efforts have been made in measuring the short-range nucleon–nucleon correlation and extracting the ratio of nucleons in the high-momentum tail experimentally [46–50] and theoretically [51, 52] (see, e.g., Ref. [53] for a review). In particular, it was found that the neutron-proton correlation is much stronger than the correlation between neutron-neutron and proton-proton pairs [48–50], and this is mainly due to the nuclear tensor force. The isospin dependence of the short-range correlation can lead to interesting consequences, such as the reduction of the kinetic contribution to the nuclear symmetry energy [54–56] compared to the free Fermi gas scenario. Because the symmetry energy at saturation density is constrained to be around 30 MeV from many analyses (see, e.g., Ref. [57]), the isospin-dependent short-range correlation effectively increases the potential contribution to the symmetry energy and thus the symmetry potential effect, which may lead to enhanced isospin effects

in intermediate-energy HICs [58, 59].

3 Spin in nuclear reactions

The spin Hall effect was first predicted by Dyakonov and Perel in 1971 [6, 7], while the term spin Hall effect was coined by Hirsch in 1999 [5]. Given the transport of spin-up and spin-down particles with spin–orbit coupling, i.e., $U^{so} = -\boldsymbol{L}\cdot\boldsymbol{\sigma}$ with $\boldsymbol{L}$ being the angular momentum and $\boldsymbol{\sigma}$ being the particle spin, the spin-up (spin-down) particles tend to turn left (right) to couple with the angular momentum and lower the energy, leading to the splitting of final observables for different spin states, as shown in Fig. 1. In this section, we will discuss similar effects in low- and intermediate-energy HICs based on the framework of TDHF, BUU, and QMD, with more complicated forms of spin–orbit coupling from spin-dependent nuclear interactions.

3.1 TDHF model study

The mean-field dynamics of nucleons in the TDHF model is described by

$$\mathrm{i}\frac{\partial}{\partial t}\phi_i = h\phi_i, \tag{14}$$

where ϕ_i is the wave function of the ith nucleon and the single-nucleon Hamlitonian is given by

$$h\phi_i = \frac{\delta E}{\delta \phi_i^\star}, \tag{15}$$

with E being the energy functional of the nuclear system from the Hartree-Fock calculation. The single-nucleon Hamiltonian is generally a function of nucleon number density ρ, spin density $\boldsymbol{s}$, current density $\boldsymbol{j}$, spin-current density $\boldsymbol{J}$, and so on, and their definitions in terms of the nucleon wave function are

$$\rho = \sum_i \phi_i^\star \phi_i, \tag{16}$$

$$\boldsymbol{s} = \sum_i \sum_{\sigma,\sigma'} \phi_i^\star \langle\sigma|\boldsymbol{\sigma}|\sigma'\rangle \phi_i, \tag{17}$$

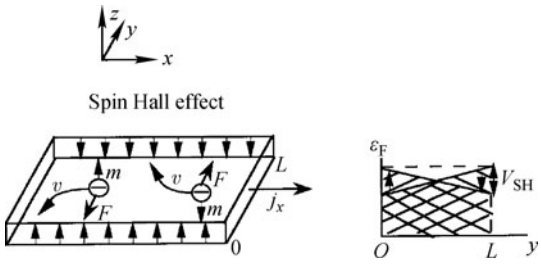

Fig. 1 Schematic of the spin Hall effect. Figure taken from Ref. [5].

$$\boldsymbol{j} = \frac{1}{2\mathrm{i}}\sum_i (\phi_i^\star \nabla\phi_i - \phi_i \nabla\phi_i^\star), \tag{18}$$

$$\boldsymbol{J} = \frac{1}{2\mathrm{i}}\sum_i \sum_{\sigma,\sigma'} (\phi_i^\star \nabla\phi_i - \phi_i \nabla\phi_i^\star) \times \langle\sigma|\boldsymbol{\sigma}|\sigma'\rangle, \tag{19}$$

with $\langle\sigma|\boldsymbol{\sigma}|\sigma'\rangle$ being the Pauli matrix element. Numerically, these densities can be calculated on the coordinate space grid and Eq. (14) can be solved with a fixed time step. For more details, we refer the reader to Refs. [60, 61]. The TDHF framework works well for low-energy heavy-ion reactions and in studying resonances dynamics.

In the old calculations, the single-nucleon Hamiltonian was generally calculated from the SHF model without the spin–orbit interaction and time-odd terms. The spin–orbit force was first introduced to the TDHF framework in Refs. [62–64]. It is interesting to see that the spin–orbit force enhances the dissipation in the fusion reaction and transforms the relative motions of the two nuclei into the internal excitations. The fusion threshold energy in the $O^{16} + O^{16}$ reaction is increased by about a factor of 2 [62, 63], as shown in Fig. 2 with three different parameterizations of the Skyrme force. The fusion cross section obtained from the TDHF calculation was increased after including the spin–orbit force [62].

With only a time-even contribution of the spin–orbit interaction, i.e., the spin–orbit potential [Eq. (2)] and the potential with spin-current density $\boldsymbol{J}$ [Eq. (10)], spurious spin twist can be generated in a free moving nucleus, as a result of spin–orbit coupling. Obviously, this phenomenon is not reasonable as it depends on the reference frame. By considering that all kinds of collision geometry can be realized in HICs, the time-odd terms were further introduced in the TDHF calculation in Refs. [65, 66] to satisfy the invariance under Galilei transformations. It is

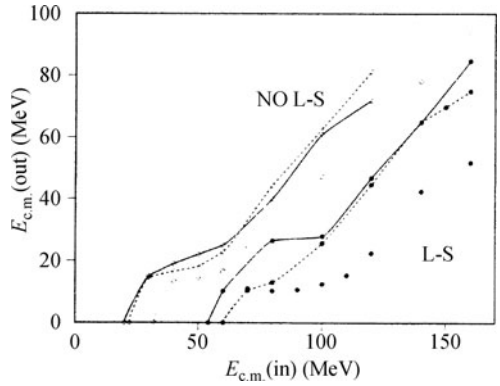

Fig. 2 Relation between the outgoing energy and incoming energy in the $O^{16} + O^{16}$ reaction from the TDHF study. The filled (open) circles are results with (without) the spin–orbit force, and the solid, dashed, and dotted curves represent results from three different Skyrme forces. Figure taken from Ref. [63].

seen from Fig. 3 that there is no such spurious spin and that the kinetic energy is a constant before 50 fm/c when the nuclei are moving freely, as a result of a suppression effect on the time-even terms from the time-odd terms. During the reaction process, the real spin twist appears owing to the overwhelming effect of the time-odd terms on the time-even terms, as shown in Fig. 4. At the end of the reaction, the energy of the outgoing nuclei is smaller with the time-odd terms, as shown in Fig. 3, indicating a stronger dissipation. Besides the spin excitation, it was found that the fusion description was further improved with the time-odd terms and the spin-current pseudotensor contribution [66]. A more detailed study on this topic done recently [67] showed that the dissipation is dominated by the time-even contribution of the spin–orbit force at lower energies but by the time-odd terms at higher energies.

Besides the spin–orbit force, the additional contribution of the spin-current density $\boldsymbol{J}$ was introduced in the TDHF calculation to represent the contribution from the tensor force in Ref. [68]. It was found that the dissipation effect from the tensor force is small compared with that from the spin–orbit force [68, 69]. However, the spin

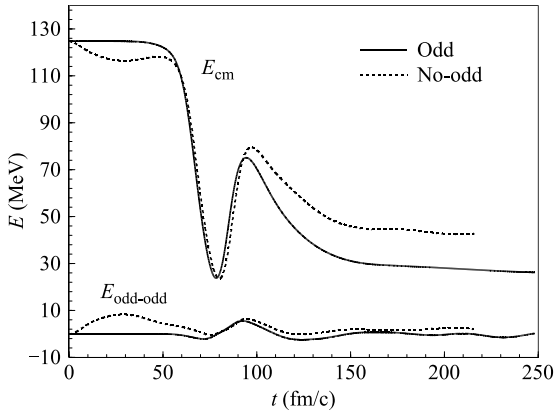

Fig. 3 Center-of-mass energy evolution in central $O^{16} + O^{16}$ reactions with (solid lines) and without (dashed lines) time-odd contributions from the TDHF calculation. The time window of the reaction process is from about 50 to 120 fm/c. Figure taken from Ref. [65].

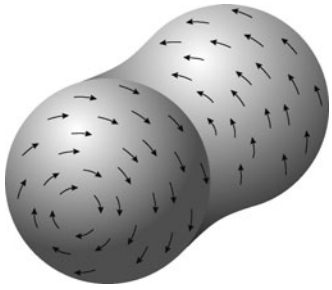

Fig. 4 Spin excitation in central $O^{16} + O^{16}$ reactions from the TDHF study with both time-even and time-odd terms. Figure taken from Ref. [65].

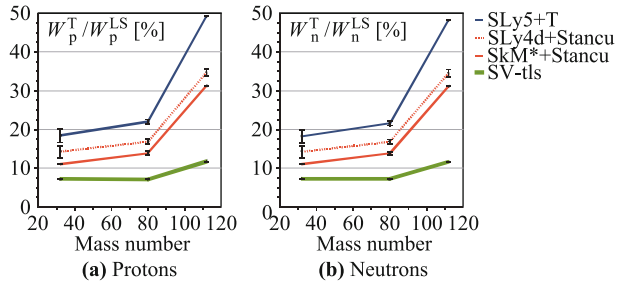

Fig. 5 Ratios of the spin mean field from the spin-current density representing the tensor force to that from the spin–orbit force for protons **(a)** and neutrons **(b)** as a function of the mass of the reaction nuclei. Different parameterizations of the Skyrme force are used in the study. Figure taken from Ref. [68].

mean field can be enhanced with the nuclear tensor force, and the enhancement becomes important with the increasing mass of the colliding nuclei, as shown in Fig. 5, depending on the parameterization of the Skyrme force. A more complete study including the full Skyrme functional as well as the tensor force in the TDHF calculation was done very recently in Ref. [70]. It was found that the Skyrme tensor force has non-negligible effects on low-energy heavy-ion dynamics and the fusion threshold energy.

3.2 BUU model study

The TDHF model works well in low-energy HICs, but the particle emission and nucleon–nucleon scattering are still lacking. To describe these effects in intermediate-energy HICs, BUU models and QMD models are suitable candidates. In the BUU framework, the Boltzmann equation is solved with the test particle method [71, 72]. In previous studies, an isospin-dependent BUU (IBUU) transport model has been used to describe the isospin dynamics in intermediate-energy HICs [3]. Recently, the spin degree of freedom of nucleons and the spin–orbit interaction were incorporated into the IBUU model, and the new model is dubbed as the spin- and isospin-dependent BUU (SIBUU) model [73–77]. In this section, we summarize the main results published originally in Refs. [73–77].

In the SIBUU model, each nucleon is assigned randomly a unit vector representing the expectation value of its spin. In this way, the spin projection of each nucleon in an arbitrary direction can be easily calculated. In the transport simulation, the z direction is set as the beam momentum and the x direction is for the impact parameter. Since the total angular momentum in non-central HICs is in the y direction perpendicular to the reaction plane, i.e., the x-O-z plane, it is reasonable to study the spin polarization in the y direction. We thus

determine the nucleons with spin projection on $+y$ $(-y)$ direction as the spin-up (spin-down) nucleons.

Considering the general form of the time-even and time-odd spin-dependent potentials in Eqs. (11) and (12), one can describe the time evolutions of the coordinate, momentum, and spin degrees of freedom by

$$\frac{\mathrm{d}\boldsymbol{r}}{\mathrm{d}t} = \frac{\boldsymbol{p}}{m} + \frac{W_0}{2}\left(\frac{\rho}{\rho_0}\right)^{\gamma}\boldsymbol{\sigma}\times(a\nabla\rho_q + b\nabla\rho_{q'}) - \frac{W_0}{2}\left(\frac{\rho}{\rho_0}\right)^{\gamma}\nabla\times(a\boldsymbol{s}_q + b\boldsymbol{s}_{q'}), \tag{20}$$

$$\frac{\mathrm{d}\boldsymbol{p}}{\mathrm{d}t} = -\nabla U_q - \nabla U_q^{s-even} - \nabla U_q^{s-odd}, \tag{21}$$

$$\frac{\mathrm{d}\boldsymbol{\sigma}}{\mathrm{d}t} = W_0\left(\frac{\rho}{\rho_0}\right)^{\gamma}[(a\nabla\rho_q + b\nabla\rho_{q'})\times\boldsymbol{p}]\times\boldsymbol{\sigma} - W_0\left(\frac{\rho}{\rho_0}\right)^{\gamma}[\nabla\times(a\boldsymbol{j}_q + b\boldsymbol{j}_{q'})]\times\boldsymbol{\sigma}. \tag{22}$$

One sees that the three degrees of freedom couple with each other. The number density ρ, the spin density $\boldsymbol{s}$, the current density $\boldsymbol{j}$, and the spin-current density $\boldsymbol{J}$ are calculated from the test particle method [71, 72, 74]. Because the mixing of the long-range Fock contribution and the spin interaction is a complex problem, the momentum dependence is not included in the spin-independent potential U_q for the moment. In addition, the spins of nucleons are randomized after nucleon–nucleon scattering, by approximately taking the spin flip effect into consideration [78, 79].

The time evolutions of the relevant density contours from the SIBUU calculation are displayed in Fig. 6. The gradient of number density, $\nabla\rho$, and the curl of the current density, $\boldsymbol{j}$, show the strength of the time-even and time-odd spin-dependent potential, respectively, and both of them are closely related to the evolution of the number density shown in the first row of Fig. 6. The nucleon spin tends to be parallel to $\boldsymbol{p}\times\nabla\rho$ from the time-even potential [Eq. (11)], whereas it tends to be parallel to $\nabla\times\boldsymbol{j}$ from the time-odd potential [Eq. (12)]. The contributions from the time-even and time-odd potentials are opposite to each other. One sees that before the two nuclei touch each other there is no spin polarization as a result of the cancellation of the time-even and time-odd potentials, consistent with the findings from TDHF studies. During the collision process, the participant is polarized in the $+y$ direction, i.e., in the direction of the total angular momentum, following the preference direction of the time-odd potential. It is seen that the direction of the spin polarization is consistent with that in Fig. 4 from the TDHF calculation with both time-even and time-odd potentials.

Transverse flow is one of the most important observables for extracting the equation of state of produced matter and studying the nuclear interaction in HICs [1, 72, 80]. The left panel of Fig. 7 displays the transverse flow of spin-up and spin-down nucleons as a function of reduced rapidity y_r/y_r^{beam}. We note that the target (projectile) nucleus is in the $+x$ $(-x)$ direction in Fig. 6, which is different from the conventional initialization, leading to the negative slope of the transverse flow. However, this does not prevent the reader from seeing the obvious splitting of transverse flow between spin-up and spin-down nucleons. With a detailed orientation analysis, one can find that again the time-odd potential dominates the effect, giving the spin-up (spin-down) nucleons an attractive (repulsive) potential. This can be understood in a naive picture in which the spin-up (spin-down) nucleons are parallel (antiparallel) to the direction of total angular momentum and thus feel an attractive (repulsive) potential. One can further define the spin up-down

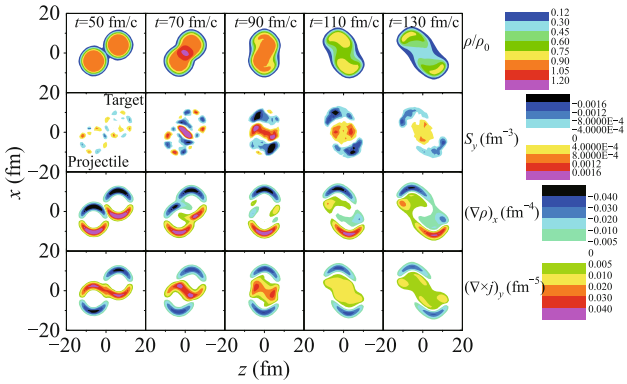

Fig. 6 Time evolution of contours of the reduced number density, ρ/ρ_0, y component of the spin density, s_y, x component of the number density gradient, $(\nabla\rho)_x$, and y component of the curl of the current density, $(\nabla\times\boldsymbol{j})_y$, in noncentral Au + Au collisions at a beam energy of 50 MeV. Figure taken from Ref. [73].

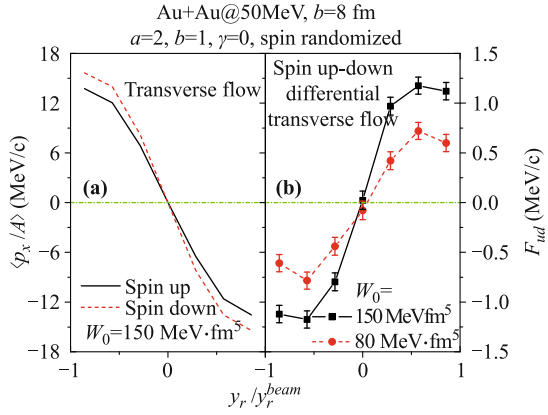

Fig. 7 Transverse flow of spin-up and spin-down nucleons **(a)** and the spin up-down differential transverse flow **(b)** with different strength of the spin–orbit coupling in noncentral Au + Au collisions at a beam energy of 50 MeV. Figure taken from Ref. [73].

differential transverse flow as follows:

$$F_{ud}(y_r) = \frac{1}{N(y_r)} \sum_{i=1}^{N(y_r)} \sigma_i(p_x)_i, \tag{23}$$

where σ_i is 1 for spin-up nucleons and -1 for spin-down nucleons, and $N(y_r)$ is the number of nucleons at rapidity y_r. The above spin up-down differential transverse flow largely cancels the effect from the spin-independent nuclear interaction while preserving the information of the spin-dependent potential. Indeed, the slope of F_{ud} increases with increasing spin–orbit coupling constant, indicating that it is a good probe of the nuclear spin-dependent interaction.

The spin up-down differential transverse flow was further analyzed in detail in Ref. [74]. Figure 8 displays the dependence of F_{ud} on the beam energy and the centrality. At higher beam energies, the angular momentum is larger while the nucleon–nucleon scattering is more violent, with the former enhancing the spin-dependent potential and the latter washing out part of the information of spin dynamics. The competition leads to a maximum slope of F_{ud} at a beam energy of ∼100 MeV, as shown in the left panel of Fig. 8. Since the spin-dependent potential is related to the density gradient and is thus a surface effect, the slope of F_{ud} increases with the increasing value of the impact parameter, as shown in the right panel of Fig. 8.

In the neutron-rich collision system where the relevant neutron densities are larger than proton densities, the difference of the spin up-down differential transverse flow of neutrons and protons can be useful to probe the isospin dependence of the spin–orbit coupling in HICs. The analysis was performed with a stronger isospin-like coupling ($a = 2$, $b = 1$) and a stronger isospin-unlike coupling ($a = 1$, $b = 2$), and the resulting F_{ud} values were calculated at different beam energies as shown in Fig. 9. A stronger isospin-like spin–orbit coupling, which

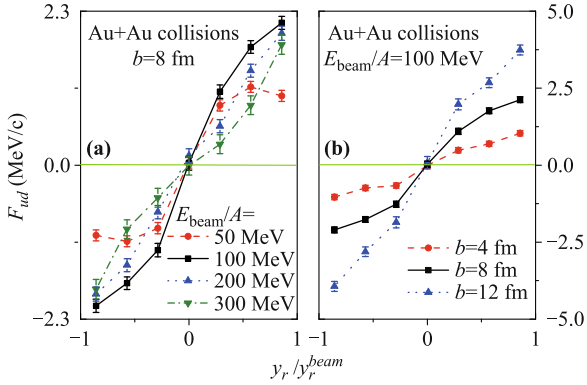

Fig. 8 Dependence of the spin up-down differential transverse flow on the beam energy **(a)** and the impact parameter **(b)** in noncentral Au + Au collisions. Figure taken from Ref. [74].

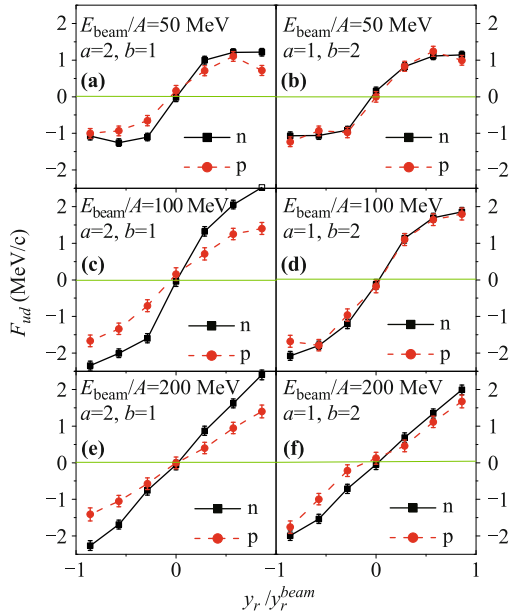

Fig. 9 Spin up-down differential transverse flow of neutrons and protons at different beam energies and with two typical isospin dependencies of the spin–orbit coupling. Figure taken from Ref. [74].

is exactly the case of the SHF interaction, leads to a larger F_{ud} for neutrons than for protons, while a stronger isospin-unlike coupling gives opposite predictions or similar F_{ud} for neutrons and protons. The effect is appreciable from beam energies of 50 to 200 MeV, with a beam energy of 100 MeV being optimal because it gives the largest magnitude of F_{ud}.

The density dependence of the spin–orbit coupling has bothered many nuclear physicists and hampered our understanding of the nuclear spin–orbit interaction in nuclear structure studies. Because HICs enable us to construct systems with designed density, isospin, and momentum current, they might be helpful in extracting useful information of the density dependence of the spin–orbit coupling. As is known, nucleons of high transverse momentum (p_T) are emitted early from the high-density phase in HICs, and the density of the high-density phase increases with increasing beam energy. This feature can be used to extract the density dependence of the spin–orbit coupling, as illustrated in Fig. 10. Without a high-p_T cut, the slope of F_{ud} can hardly be distinguished, as shown in the left panel of Fig. 10, because nucleon emission from the low-density phase, which is similar at different beam energies, dominates the results. With a high-p_T cut, the slope of F_{ud} is smaller at lower collision energies but larger at higher collision energies from a linearly increasing spin–orbit coupling strength, compared to the case with a constant one. In this way, the strength and the density dependence of the spin–orbit coupling can be disentangled.

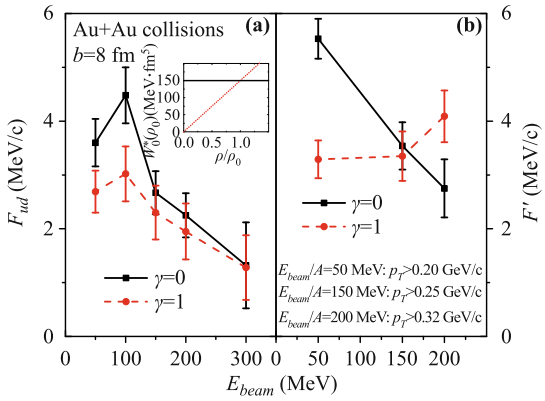

Fig. 10 Slope parameter of the spin up-down differential transverse flow F' without **(a)** and with **(b)** high transverse momentum cut from different density dependencies of the spin–orbit coupling at different beam energies. Figure taken from Ref. [74].

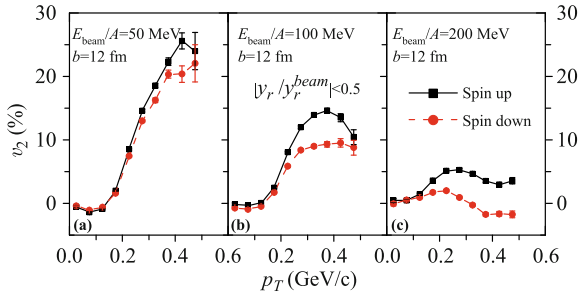

Fig. 11 Transverse momentum dependence of the elliptic flow of mid-rapidity nucleons in peripheral Au + Au collisions at different beam energies. Figure taken from Ref. [75].

In noncentral HICs, the azimuthal distribution of emitted nucleons can always be expressed as

$$E\frac{\mathrm{d}^3N}{\mathrm{d}p^3} = \frac{\mathrm{d}^2N}{2\pi p_T \mathrm{d}p_T \mathrm{d}y_r}[1 + 2v_1(y_r, p_T)\cos(\phi) + 2v_2(y_r, p_T)\cos(2\phi) + \cdots] \quad (24)$$

with $\phi = \arctan(p_y/p_x)$ being the azimuthal angle, and $v_1 = \langle\cos(\phi)\rangle$ and $v_2 = \langle\cos(2\phi)\rangle$ being called the directed flow and elliptic flow, respectively. The directed flow is similar to the transverse flow, but it depends on the flow angle rather than magnitude. The elliptic flow is positive at lower energies, is negative at intermediate energies, and becomes positive again at higher energies. Positive elliptic flow means more particles move in-plane than out-of-plane as a result of hydrodynamics, whereas negative elliptic flow is a result of the squeeze-out effect on the expansion of participant matter by the spectator nucleons [1]. Despite the complicated dynamics, the elliptic flow serves as a useful probe of the properties of nuclear matter formed in HICs and the nuclear interaction. The transverse momentum dependence of v_2 of spin-up and spin-down nucleons at mid-rapidity is displayed in Fig. 11. Except for the different behaviors of v_2 at different beam energies, a larger elliptic flow of spin-up nucleons than spin-down nucleons is observed, especially at higher transverse momentum, as a result of the stronger spin–orbit coupling for energetic nucleons. At the energy range considered, a more attractive mean-field potential leads to a larger v_2 in peripheral HICs, consistent with the effect of a spin-dependent potential on the spin splitting of transverse flow discussed above.

The above observables are for free nucleons. Experimentally, it is easier to detect charged particles rather than neutrons, leading to difficulties of measuring the spin splitting of transverse flows for protons and neutrons and identifying the isospin dependence of the spin–orbit coupling. Of course, the spin measurement poses another challenge, as will be discussed in the next section. Once the corresponding detectors are set up, the spin splitting of observables for charged light clusters may be more easily measured. For transport models with point-like particles, the dynamical coalescence approach has been shown to be successful in studying the hadronization in relativistic HICs [81, 82] and light cluster formation in intermediate-energy HICs [83, 84]. In this approach, the probability for nucleons to form a light cluster is proportional to the nucleon Wigner function of the light cluster [83, 84], and the proportional constant is the statistical factor determined by the spin-isospin degeneracy. For example, with explicit knowledge of the isospin of nucleons, the statistical factor for a neutron and a proton to form a deuteron is 3/8, whereas that for one neutron and two protons to form a ^{3}He nucleus is 1/12. Because the spin of each nucleon is also explicitly known, the dynamical coalescence can be further improved by considering the antisymmetrization of the product of spin and isospin wave function. For example, the statistical factor for a spin-up neutron and a spin-up proton to form a spin-up deuteron is 1/2, whereas for a spin-up neutron, a spin-up proton, and a spin-down proton to form a spin-up ^{3}He nucleus it is 1/2. This improvement has been applied to study spin splitting observables for deuterons, tritons, and ^{3}He nuclei [85]. It has been checked that, after spin averaging, the results reproduce those without an explicit spin treatment.

Figure 12 displays the spin splitting of the directed flows for deuterons, tritons, and ^{3}He nuclei in noncentral Au + Au collisions at a beam energy of 100 MeV. The directed flow of spin-down clusters is larger than that of spin-up ones. The spin splitting of the directed flow is largest for the deuteron owing to its large spin quantum number, i.e., $S = 1$. The spin splitting observables of tritons and ^{3}He nuclei might be more easily measurable for extracting the isospin dependence of the spin–orbit

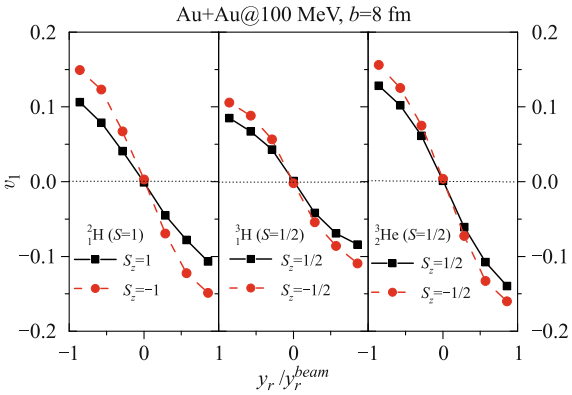

Fig. 12 Directed flow of deuterons, tritons, and ^{3}He nuclei of different spin states in noncentral Au + Au collisions at a beam energy of 100 MeV. s_z represents the spin state projecting on the y direction perpendicular to the reaction plane. Figure taken from Ref. [85].

coupling experimentally.

The elliptic flow of different spin states of deuterons in noncentral Au + Au collisions at a beam energy of 100 MeV is illustrated in Fig. 13. It is seen that the elliptic flow of spin-down deuterons is more negative at mid-rapidity, but it is slightly positive at large rapidity, indicating an obvious spin splitting even with the statistical error taken into account. Again, the magnitude of v_2 as well as its spin splitting for deuterons is larger than that of free nucleons according to Ref. [75], and it might serve as a better spin-dependent observable.

A further preliminary calculation with the full Skyrme functional has been done. A standard Skyrme functional with MSL0 parameterization [86] has been used in the calculation. The detailed derivation and expression of the full Skyrme functional with both time-even and time-odd terms can be found in Refs. [27, 29, 30]. The resulting spin up-down differential transverse flow is shown in the left panel of Fig. 14. One can see the similar sensitivity of F_{ud} to the spin–orbit coupling strength, although the

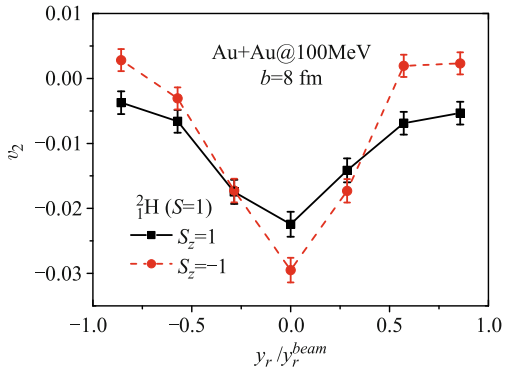

Fig. 13 Elliptic flow of spin-up and spin-down deuterons in noncentral Au + Au collisions at a beam energy of 100 MeV. s_z represents the spin state projecting on the y direction perpendicular to the reaction plane. Figure taken from Ref. [85].

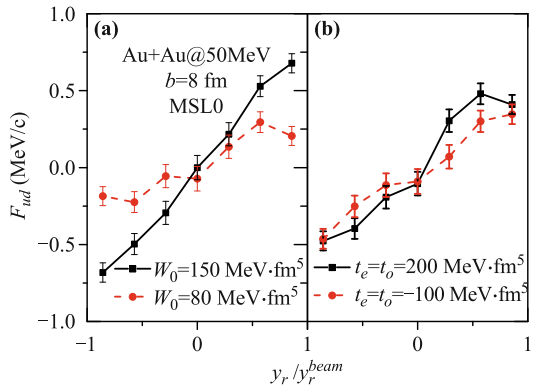

Fig. 14 Spin up-down differential transverse flow from full Skyrme calculation using the MSL0 force without **(a)** and with the tensor force **(b)**. Figure taken from Ref. [85].

magnitude is a little smaller, compared to the result shown in Fig. 7 where only the spin–orbit coupling is applied. To investigate the effect of the nuclear tensor force on the spin dynamics of intermediate-energy HICs, a zero-range tensor force of the form

$$\begin{aligned} v_t(\boldsymbol{r}) = \frac{t_e}{2}\{&[3(\boldsymbol{\sigma}_1\cdot\boldsymbol{k}')(\boldsymbol{\sigma}_2\cdot\boldsymbol{k}') - (\boldsymbol{\sigma}_1\cdot\boldsymbol{\sigma}_2)k'^2]\delta(\boldsymbol{r}) \\ &+\delta(\boldsymbol{r})[3(\boldsymbol{\sigma}_1\cdot\boldsymbol{k})(\boldsymbol{\sigma}_2\cdot\boldsymbol{k}) - (\boldsymbol{\sigma}_1\cdot\boldsymbol{\sigma}_2)k^2]\} \\ &+t_o[3(\boldsymbol{\sigma}_1\cdot\boldsymbol{k}')\delta(\boldsymbol{r})(\boldsymbol{\sigma}_2\cdot\boldsymbol{k}) - (\boldsymbol{\sigma}_1\cdot\boldsymbol{\sigma}_2)\boldsymbol{k}'\cdot\delta(\boldsymbol{r})\boldsymbol{k}] \quad (25) \end{aligned}$$

is incorporated into the full Skyrme transport model calculation, where $\boldsymbol{r} = \boldsymbol{r}_1 - \boldsymbol{r}_2$ is the relative coordinate, $\boldsymbol{k}$ and $\boldsymbol{k}'$ are the relative momentum operator and its complex conjugate, respectively, and t_e and t_o are the triplet-even and triplet-odd strength parameters, respectively. The energy-density functional derived from the above tensor force can be found in Refs. [27, 29], where the corresponding terms (such as the spin-current density $\boldsymbol{J}$) are non-negligible only when local spin polarization is produced. The resulting spin up-down differential transverse flow is shown in the right panel of Fig. 14. It is seen that the slope of F_{ud} is not very sensitive to the values of t_e or t_o unless an extremely large coupling constant is used. This feature is consistent with the TDHF study where the spin dynamics is dominated by the spin–orbit coupling. However, one would expect that, with a spin-polarized beam or target, the tensor force effect can be much enhanced.

3.3 QMD model study

In the QMD framework, the Wigner function of each nucleon is treated as a Gaussian wave packet in both coordinate and momentum space [87, 88], and the two-nucleon interaction is related to the effective two-body interaction and the overlap of their wave functions. The

equation of motion in the QMD model is given by the semiclassical canonical equation, i.e.,

$$\frac{\mathrm{d}\boldsymbol{r}}{\mathrm{d}t} = \nabla_p H,$$
$$\frac{\mathrm{d}\boldsymbol{p}}{\mathrm{d}t} = -\nabla_r H, \tag{26}$$

where $\boldsymbol{r}$ and $\boldsymbol{p}$ are, respectively, the central coordinate and momentum of the wave packet, and H is the Hamiltonian of the system including the kinetic and potential energy.

In a recent study, the nuclear spin–orbit interaction was incorporated into the ultra-relativistic QMD (UrQMD) model. The potential energy contribution of the spin–orbit interaction is expressed as [89]

$$U_s = \int u_s \mathrm{d}^3 r, \tag{27}$$

where the spin-dependent potential u_s consists of time-even and time-odd contributions written as

$$u_s^{even} = -\frac{W_0}{2}(\rho\nabla\cdot\boldsymbol{J} + \rho_n\nabla\cdot\boldsymbol{J}_n + \rho_p\nabla\cdot\boldsymbol{J}_p), \tag{28}$$

$$u_s^{odd} = -\frac{W_0}{2}[\boldsymbol{s}\cdot(\nabla\times\boldsymbol{j}) + \boldsymbol{s}_n\cdot(\nabla\times\boldsymbol{j}_n) + \boldsymbol{s}_p\cdot(\nabla\times\boldsymbol{j}_p)], \tag{29}$$

where W_0 represents the spin–orbit coupling strength, and ρ, $\boldsymbol{s}$, $\boldsymbol{j}$, and $\boldsymbol{J}$ are the number, spin, current, and spin-current densities, which can be calculated from the local Wigner function of the nucleon [89].

The spin dynamics was analyzed based on the above framework. Similar spin splittings of the directed flow and the elliptic flow were observed in noncentral Au + Au collisions at a beam energy of 150 MeV, as shown in Fig. 15. It was argued that the net spin-dependent potential is attractive for spin-up protons and repulsive for spin-down protons, leading to a larger directed flow for spin-down protons than spin-up protons. The spin splitting of p_T-integrated elliptic flow was found to be small and only visible in peripheral collisions, and it was found that v_2 for spin-down protons is slightly larger than that for spin-up ones. Since the conventional initial direction of the target and projectile is used as shown in Fig. 3 of Ref. [89], the spin-up (spin-down) nucleons correspond to the spin-down (spin-up) ones in the SIBUU study [73–77]. Although the spin splitting of final collective flow is a robust phenomenon in both models, further studies are needed to understand the relative sign of the splitting.

Further analysis was done on the beam energy dependence of the flow splitting. By defining κ_{up} and κ_{down} as the slope parameter of the directed flow of spin-up and spin-down protons, respectively, the slope difference is shown to increase with increasing impact parameter, as shown in the upper panel of Fig. 16; this is qualitatively consistent with SIBUU studies. In noncentral Au + Au collisions, it was found that the slope difference first increases then decreases with increasing beam energy, and the maximum difference appears at a beam energy of 150 MeV, similar to the finding in the SIBUU model where

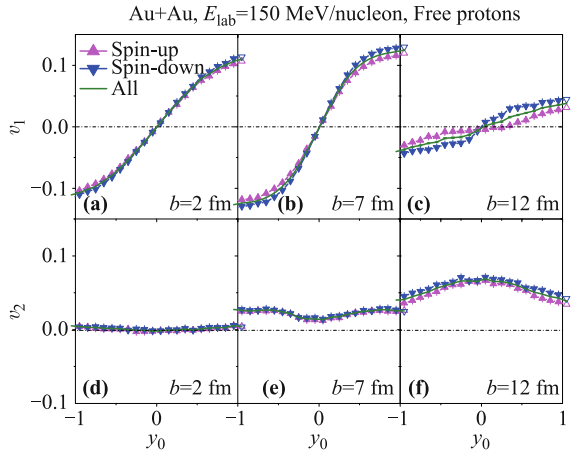

Fig. 15 The directed flow (*upper panels*) and elliptic flow (*lower panels*) for spin-up and spin-down protons in noncentral Au + Au collisions at a beam energy of 150 MeV from the QMD calculation. Figure taken from Ref. [89].

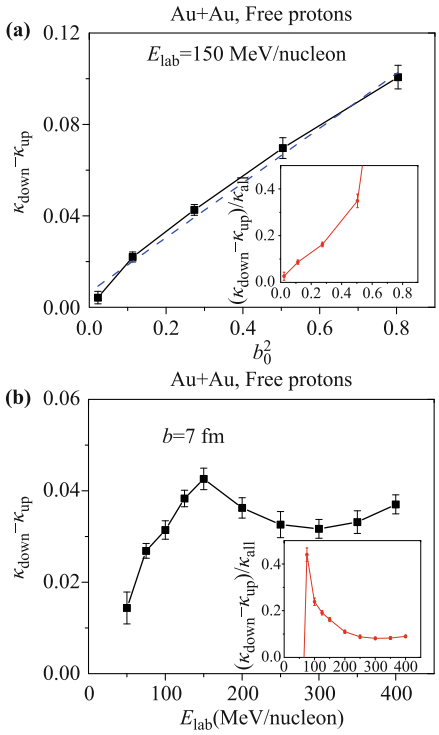

Fig. 16 Difference of the slope of directed flow between spin-up and spin-down protons as a function of impact parameter (upper panel) and beam energy (lower panel). The dashed line in the upper panel is a linear fit, while the inset in the lower panel shows the relative difference. Figure taken from Ref. [89].

the maximum slope of the spin up-down differential transverse flow appears at a beam energy of about ∼100 MeV.

It was further emphasized in Ref. [89] that the spin-averaged flow results do not change after including the spin–orbit interaction, as a result of the cancellation of spin-up and spin-down nucleons. In addition, the spin splitting of the flow slope caused by the spin–orbit interaction is comparable to the isospin splitting caused by the nuclear symmetry energy, especially for neutrons. These findings are all consistent with the observations in SIBUU studies [73–77].

4 Experimental status

Owing to the difficulties of spin measurement in HIC experiments, the main focus in the past has been mainly on the spin-averaged observables, and information on spin dynamics has been neglected. Because of the great efforts made by experimental nuclear physicists, making measurements of the spin of free nucleons and light clusters has now become possible. Although the detailed experimental status will be presented in another review of this issue, here we briefly mention two related experiments that might be relevant in analyzing the probes discussed above. One of them is the spin-polarized beam that can be produced through pick-up or removal reactions at Rikagaku Kenkyusho (RIKEN) [90, 91], Gesellschaft für Schwerionenforschung mbH (GSI) [92], the National Superconducting Cyclotron Laboratory (NSCL) [93], and the Grand Accélérateur National d'Ions Lourds (GANIL) [94–96]. It is expected that the effects of spin dynamics with a spin-polarized beam will be much enhanced, providing a better system for extracting information on the spin-dependent nuclear force, especially the nuclear tensor force. For the spin-excitation state of heavy clusters, the spin polarization and alignment can be measured via the angular distribution of its γ or β decay (see, e.g., Ref. [97] for a review). Making use of the analyzing power of a nucleus might be the most promising way of identifying the spin of free nucleons or light clusters experimentally. The analyzing power indicates the left-right scattering asymmetry of an incident polarized nucleon on the target nucleus. The spin-dependent scattering is a result of the interference of the electromagnetic interaction and the hadronic force [98], and the spin flip is observed between not only charged-charged scattering but also between charged-neutral scattering. It is noteworthy that at certain energies and scattering angles the analyzing power can be as large as 100% [99]. Experimental efforts are thus encouraged by using the selected nucleus as a "detector" whose analyzing power is known *a priori*. In this way the spin of corresponding particles can be measured and the probes discussed in the previous sections can be analyzed.

5 Summary

In summary, we outlined the major physics motivations for investigating in-medium spin-dependent nuclear interactions, i.e., the spin–orbit interaction and the nuclear tensor force, and summarized some recent efforts in exploring the spin dynamics in low- and intermediate-energy heavy-ion collisions. In particular, studies on the strength, the density, and the isospin dependence of the spin–orbit interaction as well as the short-range correlation induced by the tensor force are highlighted. In TDHF studies, it has been found that the spin–orbit interaction can enhance the dissipation in low-energy heavy-ion reactions and increase the fusion threshold. Incorporating both the time-even and time-odd contribution of the spin–orbit interaction can lead to nontrivial spin polarization, while the tensor force slightly enhances the spin field compared to the spin–orbit interaction. In studies using HICs at intermediate energies, both the spin- and isospin-dependent BUU models and QMD model predict the spin splitting of the nucleon collective flow, which seems to be a robust phenomenon. In the BUU model studies, efforts have been made in extracting the isospin dependence of the spin–orbit coupling and disentangling its strength and density dependence. Preliminary results on spin splitting of observables related to the light clusters and those from the full Skyrme calculation with a nuclear tensor force have also been discussed in the BUU model studies. We hope that the findings summarized in this review will soon stimulate more experimental work in this direction.

Acknowledgements This work was supported by the Major State Basic Research Development Program (973 Program) of China under Contract Nos. 2015CB856904 and 2014CB845401, the National Natural Science Foundation of China under Grant Nos. 11320101004, 11475243, and 11421505, the "100-Talent Plan" of Shanghai Institute of Applied Physics under Grant Nos. Y290061011 and Y526011011 from the Chinese Academy of Sciences, the "Shanghai Pujiang Program" under Grant No. 13PJ1410600, the U.S. National Science Foundation under Grant No. PHY-1068022, the U.S. Department of Energy Office of Science under Award No. DE-SC0013702, and the CUSTIPEN (China–U.S. Theory Institute for Physics with Exotic Nuclei) under the U.S. Department of Energy Grant No. DE-FG02-13ER42025.

References and notes

1. P. Danielewicz, R. Lacey, and W. G. Lynch, Determination of the equation of state of dense matter, *Science* 298(5598), 1592 (2002)
2. V. Baran, M. Colonna, V. Greco, and M. Di Toro, Reaction dynamics with exotic nuclei, *Phys. Rep.* 410(5–6), 335 (2005)
3. B. A. Li, L. W. Chen, and C. M. Ko, Recent progress and new challenges in isospin physics with heavy-ion reactions, *Phys. Rep.* 464(4–6), 113 (2008)
4. H. Liang, J. Meng, and S. G. Zhou, Hidden pseudospin and spin symmetries and their origins in atomic nuclei, *Phys. Rep.* 570, 1 (2015)
5. J. E. Hirsch, Spin Hall effect, *Phys. Rev. Lett.* 83(9), 1834 (1999)
6. M. I. Dyakonov and V. I. Perel, Possibility of orientating electron spins with current, *Sov. Phys. JETP Lett.* 13, 467 (1971)
7. M. I. Dyakonov and V. I. Perel, Current-induced spin orientation of electrons in semiconductors, *Phys. Lett. A* 35(6), 459 (1971)
8. Lecture Notes of R. Machleidt, CNS Summer School, University of Tokyo, Aug. 18–23, 2005
9. M. G. Mayer, On closed shells in nuclei, *Phys. Rev.* 74(3), 235 (1948) M. G. Mayer, On closed shells in nuclei (II), *Phys. Rev.* 75(12), 1969 (1949)
10. O. Haxel, J. H. D. Jensen, and H. E. Suess, On the "magic numbers" in nuclear structure, *Phys. Rev.* 75(11), 1766 (1949)
11. D. Vautherin and D. M. Brink, Hartree–Fock calculations with Skyrme's interaction (I): Spherical nuclei, *Phys. Rev. C* 5(3), 626 (1972)
12. P. Ring, Relativistic mean field theory in finite nuclei, *Prog. Part. Nucl. Phys.* 37, 193 (1996)
13. M. Bender, P. Heenen, and P.-G Reinhard, Self-consistent mean-field models for nuclear structure, *Rev. Mod. Phys.* 75, 121 (2003)
14. P. G. Reinhard, The relativistic mean-field description of nuclei and nuclear dynamics, *Rep. Prog. Phys.* 52(4), 439 (1989)
15. A. Sulaksono, T. Bürvenich, J. A. Maruhn, P. G. Reinhard, and W. Greiner, The nonrelativistic limit of the relativistic point coupling model, *Ann. Phys.* 308(1), 354 (2003)
16. J. M. Pearson and M. Farine, Relativistic mean-field theory and a density-dependent spin–orbit Skyrme force, *Phys. Rev. C* 50(1), 185 (1994)
17. B. G. Todd-Rutel, J. Piekarewicz, and P. D. Cottle, Spin-orbit splitting in low-j neutron orbits and proton densities in the nuclear interior, *Phys. Rev. C* 69, 021301 (2004)
18. M. Grasso, L. Gaudefroy, E. Khan, T. Nikšić, J. Piekarewicz, O. Sorlin, N. V. Giai, and D. Vretenar, Nuclear "bubble" structure in Si^{34}, *Phys. Rev. C* 79(3), 034318 (2009)
19. O. Sorlin and M. G. Porquet, Evolution of the $N = 28$ shell closure: A test bench for nuclear forces, *Phys. Scr.* T152, 014003 (2013)
20. P. G. Reinhard and H. Flocard, Nuclear effective forces and isotope shifts, *Nucl. Phys. A* 584(3), 467 (1995)
21. M. M. Sharma, G. Lalazissis, J. König, and P. Ring, Isospin dependence of the spin–orbit force and effective nuclear potentials, *Phys. Rev. Lett.* 74(19), 3744 (1995)
22. M. Onsi, R. C. Nayak, J. M. Pearson, H. Freyer, and W. Stocker, Skyrme representation of a relativistic spin–orbit field, *Phys. Rev. C* 55(6), 3166 (1997)
23. J. M. Pearson, Skyrme Hartree–Fock method and the spin–orbit term of the relativistic mean field, *Phys. Lett. B* 513(3–4), 319 (2001)
24. G. A. Lalazissis, D. Vretenar, W. Pöschl, and P. Ring, Reduction of the spin–orbit potential in light drip-line nuclei, *Phys. Lett. B* 418(1–2), 7 (1998)
25. B. S. Pudliner, A. Smerzi, J. Carlson, V. R. Pandharipande, S. C. Pieper, and D. G. Ravenhall, Neutron drops and Skyrme energy-density functionals, *Phys. Rev. Lett.* 76(14), 2416 (1996)
26. J. P. Schiffer, S. J. Freeman, J. A. Caggiano, C. Deibel, A. Heinz, C.L. Jiang, R. Lewis, A. Parikh, P. D. Parker, K. E. Rehm, S. Sinha, and J. S. Thomas, Is the nuclear spin–orbit interaction changing with neutron excess? *Phys. Rev. Lett.* 92(16), 162501 (2004) [Erratum: *Phys. Rev. Lett.*, 110, 169901 (2013)]
27. T. Lesinski, M. Bender, K. Bennaceur, T. Duguet, and J. Meyer, Tensor part of the Skyrme energy density functional: Spherical nuclei, *Phys. Rev. C* 76(1), 014312 (2007)
28. M. Zalewski, J. Dobaczewski, W. Satuła, and T. R. Werner, Spin–orbit and tensor mean-field effects on spin–orbit splitting including self-consistent core polarizations, *Phys. Rev. C* 77(2), 024316 (2008)
29. M. Bender, K. Bennaceur, T. Duguet, P. H. Heenen, T. Lesinski, and J. Meyer, Tensor part of the Skyrme energy density functional (II): Deformation properties of magic and semi-magic nuclei, *Phys. Rev. C* 80(6), 064302 (2009)
30. Y. M. Engel, D. M. Brink, K. Goeke, S. J. Krieger, and D. Vautherin, Time-dependent Hartree–Fock theory with Skyrme's interaction, *Nucl. Phys. A* 249(2), 215 (1975)
31. T. H. R. Skyrme, The effective nuclear potential, *Nucl. Phys.* 9(4), 615 (1958)
32. T. Otsuka, T. Suzuki, R. Fujimoto, H. Grawe, and Y. Akaishi, Evolution of nuclear shells due to the tensor force, *Phys. Rev. Lett.* 95(23), 232502 (2005)
33. T. Otsuka, T. Matsuo, and D. Abe, Mean field with tensor force and shell structure of exotic nuclei, *Phys. Rev. Lett.* 97(16), 162501 (2006)
34. T. Otsuka, T. Suzuki, M. Honma, Y. Utsuno, N. Tsunoda, K. Tsukiyama, and M. Hjorth-Jensen, Novel features of nuclear forces and shell evolution in exotic nuclei, *Phys. Rev. Lett.* 104(1), 012501 (2010)

35. L. Gaudefroy, O. Sorlin, D. Beaumel, Y. Blumenfeld, Z. Dombrádi, S. Fortier, S. Franchoo, M. Gélin, J. Gibelin, S. Grévy, F. Hammache, F. Ibrahim, K. W. Kemper, K. L. Kratz, S. M. Lukyanov, C. Monrozeau, L. Nalpas, F. Nowacki, A. N. Ostrowski, T. Otsuka, Y.E. Penionzhkevich, J. Piekarewicz, E. C. Pollacco, P. Roussel-Chomaz, E. Rich, J. A. Scarpaci, M. G. St. Laurent, D. Sohler, M. Stanoiu, T. Suzuki, E. Tryggestad, and D. Verney, Reduction of the spin–orbit splittings at the $N=28$ shell closure, *Phys. Rev. Lett.* 97(9), 092501 (2006)

36. G. Colò, H. Sagawa, S. Fracasso, and P. F. Bortignon, Spin–orbit splitting and the tensor component of the Skyrme interaction, *Phys. Lett. B* 646(5–6), 227 (2007) [Erratum: *Phys. Lett. B*, 668, 457 (2008)].

37. L. G. Cao, G. Colò, H. Sagawa, P. F. Bortignon, and L. Sciacchitano, Effects of the tensor force on the multipole response in finite nuclei, *Phys. Rev. C* 80(6), 064304 (2009)

38. C. L. Bai, H. Q. Zhang, H. Sagawa, X. Z. Zhang, G. Coló, and F. R. Xu, Effect of the tensor force on the charge exchange spin-dipole excitations of Pb^{208}, *Phys. Rev. Lett.* 105(7), 072501 (2010)

39. C. L. Bai, H. Q. Zhang, H. Sagawa, X. Z. Zhang, G. Coló, and F. R. Xu, Spin-isospin excitations as quantitative constraints for the tensor force, *Phys. Rev. C* 83(5), 054316 (2011)

40. E. B. Suckling and P. D. Stevenson, The effect of the tensor force on the predicted stability of superheavy nuclei, *Eur. Phys. Lett.* 90(1), 12001 (2010)

41. H. A. Bethe, Theory of nuclear matter, *Annu. Rev. Nucl. Part. Sci.* 21(1), 93 (1971)

42. V. R. Pandharipande, Variational calculation of nuclear matter, *Nucl. Phys. A* 181(1), 33 (1972)

43. S. Fantoni and V. R. Pandharipande, Momentum distribution of nucleons in nuclear matter, *Nucl. Phys. A* 427(3), 473 (1984)

44. S. C. Pieper, R. B. Wiringa, and V. R. Pandharipande, Variational calculation of the ground state of O^{16}, *Phys. Rev. C* 46(5), 1741 (1992)

45. C. Ciofi degli Atti and S. Simula, Realistic model of the nucleon spectral function in few- and many-nucleon systems, *Phys. Rev. C* 53(4), 1689 (1996)

46. A. Tang, J. W. Watson, J. Aclander, J. Alster, G. Asryan, Y. Averichev, D. Barton, V. Baturin, N. Bukhtoyarova, A. Carroll, S. Gushue, S. Heppelmann, A. Leksanov, Y. Makdisi, A. Malki, E. Minina, I. Navon, H. Nicholson, A. Ogawa, Y. Panebratsev, E. Piasetzky, A. Schetkovsky, S. Shimanskiy, and D. Zhalov, $n-p$ short-range correlations from $(p, 2p+n)$ measurements, *Phys. Rev. Lett.* 90(4), 042301 (2003)

47. K. S. Egiyan, et al. (CLAS Collaboration), Measurement of two- and three-nucleon short-range correlation probabilities in nuclei, *Phys. Rev. Lett.* 96(8), 082501 (2006)

48. E. Piasetzky, M. Sargsian, L. Frankfurt, M. Strikman, and J. W. Watson, Evidence for strong dominance of proton-neutron correlations in nuclei, *Phys. Rev. Lett.* 97(16), 162504 (2006)

49. R. Subedi, R. Shneor, P. Monaghan, B. D. Anderson, K. Aniol, J. Annand, J. Arrington, H. Benaoum, F. Benmokhtar, W. Boeglin, et al., Probing cold dense nuclear matter, *Science* 320(5882), 1476(2008)

50. O. Hen, et al. (Jefferson Lab CLAS Collaboration), Momentum sharing in imbalanced Fermi systems, *Science* 346(6209), 614 (2014)

51. R. Schiavilla, R. B. Wiringa, S. C. Pieper, and J. Carlson, Tensor forces and the ground-state structure of nuclei, *Phys. Rev. Lett.* 98(13), 132501 (2007)

52. M. Alvioli, C. Ciofi degli Atti, and H. Morita, Proton-neutron and proton-proton correlations in medium-weight nuclei and the role of the tensor force, *Phys. Rev. Lett.* 100(16), 162503 (2008)

53. J. Arrington, D. W. Higinbotham, G. Rosner, and M. Sargsian, Hard probes of short-range nucleon–nucleon correlations, *Prog. Part. Nucl. Phys.* 67(4), 898 (2012)

54. I. Vidaña, A. Polls, and C. Providencia, Nuclear symmetry energy and the role of the tensor force, *Phys. Rev. C* 84, 062801(R) (2011)

55. A. Carbone, A. Polls, and A. Rios, High-momentum components in the nuclear symmetry energy, *Eur. Phys. Lett.* 97(2), 22001 (2012)

56. C. Xu, A. Li, and B. A. Li, Delineating effects of tensor force on the density dependence of nuclear symmetry energy, *J. Phys.: Conf. Ser.* 420, 012090 (2013)

57. K. Pomorski and J. Dudek, Nuclear liquid-drop model and surface-curvature effects, *Phys. Rev. C* 67(4), 044316 (2003)

58. O. Hen, B. A. Li, W. J. Guo, L. B. Weinstein, and E. Piasetzky, Symmetry energy of nucleonic matter with tensor correlations, *Phys. Rev. C* 91(2), 025803 (2015)

59. B. A. Li, W. J. Guo, and Z. Z. Shi, Effects of the kinetic symmetry energy reduced by short-range correlations in heavy-ion collisions at intermediate energies, *Phys. Rev. C* 91(4), 044601 (2015)

60. P. Hoodbhoy and J. W. Negele, Solution of Hartree-Fock equations in coordinate space for axially symmetric nuclei, *Nucl. Phys. A*. 288(1), 23 (1977)

61. K. T. R. Davies and S. E. Koonin, Skyrme-force time-dependent Hartree–Fock calculations with axial symmetry, *Phys. Rev. C* 23(5), 2042 (1981) [Erratum: *Phys. Rev. C*, 24, 1820 (1981)]

62. A. S. Umar, M. R. Strayer, and P. G. Reinhard, Resolution of the fusion window anomaly in heavy-ion collisions, *Phys. Rev. Lett.* 56(26), 2793 (1986)

63. P. G. Reinhard, A. S. Umar, K. T. R. Davies, M. R. Strayer, and S. J. Lee, Dissipation and forces in time-dependent Hartree-Fock calculations, *Phys. Rev. C* 37(3), 1026 (1988)

64. A. S. Umar, M. R. Strayer, P. G. Reinhard, K. T. R. Davies, and S. J. Lee, Spin–orbit force in time-dependent Hartree-Fock calculations of heavy-ion collisions, *Phys. Rev. C* 40(2), 706 (1989)

65. J. A. Maruhn, P.G. Reinhard, P. D. Stevenson, and M. R. Strayer, Spin-excitation mechanisms in Skyrme-force time-dependent Hartree-Fock calculations, *Phys. Rev. C* 74(2), 027601 (2006)
66. A. S. Umar and V. E. Oberacker, Three-dimensional unrestricted time-dependent Hartree–Fock fusion calculations using the full Skyrme interaction, *Phys. Rev. C* 73(5), 054607 (2006)
67. G. F. Dai, L. Guo, E. G. Zhao, and S. G. Zhou, Dissipation dynamics and spin–orbit force in time-dependent Hartree–Fock theory, *Phys. Rev. C* 90(4), 044609 (2014)
68. Y. Iwata and J. A. Maruhn, Enhanced spin-current tensor contribution in collision dynamics, *Phys. Rev. C* 84(1), 014616 (2011)
69. G. F. Dai, L. Guo, E. G. Zhao, and S. G. Zhou, Effect of tensor force on dissipation dynamics in time-dependent Hartree–Fock theory, *Science China-Physics, Mechanics & Astronomy* 57(9), 1618 (2014)
70. P. D. Stevenson, E. B. Suckling, S. Fracasso, M. C. Barton, and A. S. Umar, The Skyrme tensor force in heavy ion collisions, arXiv: 1507.00645 [nucl-th]
71. C. Y. Wong, Dynamics of nuclear fluid (VIII): Time-dependent Hartree–Fock approximation from a classical point of view, *Phys. Rev. C* 25(3), 1460 (1982)
72. G. F. Bertsch and S. Das Gupta, A guide to microscopic models for intermediate energy heavy ion collisions, *Phys. Rep.* 160(4), 189 (1988)
73. J. Xu and B. A. Li, Probing in-medium spin–orbit interaction with intermediate-energy heavy-ion collisions, *Phys. Lett. B* 724(4–5), 346 (2013)
74. Y. Xia, J. Xu, B. A. Li, and W. Q. Shen, Spin–orbit coupling and the up-down differential transverse flow in intermediate-energy heavy-ion collisions, *Phys. Rev. C* 89(6), 064606 (2014)
75. Y. Xia, J. Xu, B. A. Li, and W. Q. Shen, The spin-splitting of collective flows in intermediate-energy heavy-ion collisions, arXiv: 1411.3057 [nucl-th]
76. J. Xu, B. A. Li, Y. Xia, and W. Q. Shen, Spin Effects in Intermediate-energy Heavy-ion Collisions, *Nucl. Phys. Rev.* 31, 306 (2014)
77. J. Xu, Y. Xia, B. A. Li, and W. Q. Shen, Spin-orbit coupling in intermediate-energy heavy-ion collisions, *Nucl. Technol.* 37, 100513 (2014) (in Chinese)
78. G. G. Ohlsen, Polarization transfer and spin correlation experiments in nuclear physics, *Rep. Prog. Phys.* 35(2), 717 (1972)
79. W. G. Love and M. A. Franey, Effective nucleon–nucleon interaction for scattering at intermediate energies, *Phys. Rev. C* 24(3), 1073 (1981); W. G. Love and M. A. Franey, Erratum: Effective nucleon–nucleon interaction for scattering at intermediate energies, *Phys. Rev. C* 27(1), 438 (1983)
80. P. Danielewicz and G. Odyniec, Transverse momentum analysis of collective motion in relativistic nuclear collisions, *Phys. Lett. B* 157(2–3), 146 (1985)
81. V. Greco, C. M. Ko, and P. Lévai, Parton coalescence and the antiproton/pion anomaly at RHIC, *Phys. Rev. Lett.* 90(20), 202302 (2003)
82. V. Greco, C. M. Ko, and P. Lévai, Partonic coalescence in relativistic heavy ion collisions, *Phys. Rev. C* 68(3), 034904 (2003)
83. L. W. Chen, C. M. Ko, and B. A. Li, Light cluster production in intermediate energy heavy-ion collisions induced by neutron-rich nuclei, *Nucl. Phys. A* 729(2–4), 809 (2003)
84. L. W. Chen, C. M. Ko, and B. A. Li, Light clusters production as a probe to nuclear symmetry energy, *Phys. Rev. C* 68(1), 017601 (2003)
85. Y. Xia, J. Xu, B. A. Li, and W. Q. Shen, in preparation.
86. L. W. Chen, C. M. Ko, B. A. Li, and J. Xu, Density slope of the nuclear symmetry energy from the neutron skin thickness of heavy nuclei, *Phys. Rev. C* 82(2), 024321 (2010)
87. C. Hartnack, L. Zhuxia, L. Neise, G. Peilert, A. Rosenhauer, H. Sorge, J. Aichelin, H. Stöcker, and W. Greiner, Quantum molecular dynamics a microscopic model from UNILAC to CERN energies, *Nucl. Phys. A*. 495(1–2), 303 (1989)
88. J. Aichelin, "Quantum" molecular dynamics — a dynamical microscopic n-body approach to investigate fragment formation and the nuclear equation of state in heavy ion collisions, *Phys. Rep.* 202(5–6), 233 (1991)
89. C. C. Guo, Y. J. Wang, Q. F. Li, and F. S. Zhang, Effect of the spin–orbit interaction on flows in heavy-ion collisions at intermediate energies, *Phys. Rev. C* 90(3), 034606 (2014)
90. K. Asahi, M. Ishihara, N. Inabe, T. Ichihara, T. Kubo, M. Adachi, H. Takanashi, M. Kouguchi, M. Fukuda, D. Mikolas, D. J. Morrissey, D. Beaumel, T. Shimoda, H. Miyatake, and N. Takahashi, New aspect of intermediate energy heavy ion reactions. Large spin polarization of fragments, *Phys. Lett. B* 251(4), 488 (1990)
91. H. Okuno, K. Asahi, H. Sato, H. Ueno, J. Kura, M. Adachi, T. Nakamura, T. Kubo, N. Inabe, A. Yoshida, T. Ichihara, Y. Kobayashi, Y. Ohkubo, M. Iwamoto, F. Ambe, T. Shimoda, H. Miyatake, N. Takahashi, J. Nakamura, D. Beaumel, D. J. Morrissey, W. D. Schmidt-Ott, and M. Ishihara, Systematic behavior of ejectile spin polarization in the projectile fragmentation reaction, *Phys. Lett. B* 335(1), 29 (1994)
92. W.-D. Schmidt-Ott, K. Asahi, Y. Fujita, H. Geissel, K.-D. Gross, T. Hild, H. Irnich, M. Ishihara, K. Krumbholz, V. Kunze, A. Magel, F. Meissner, K. Muto, F. Nickel, H. Okuno, M. Pfützner, C. Scheidenberger, K. Suzuki, M. Weber, C. Wennemann, Spin alignment of ^{43}Sc produced in the fragmentation of 500 MeV/u ^{46}Ti, *Z. Phys. A* 350(3), 215 (1994)
93. D. E. Groh, P. F. Mantica, A. E. Stuchbery, A. Stolz, T. J. Mertzimekis, W. F. Rogers, A. D. Davies, S. N. Liddick, and B. E. Tomlin, Spin polarization of K^{37} produced in a single-proton pickup reaction at intermediate energies, *Phys. Rev. Lett.* 90(20), 202502 (2003)

94. K. Asahi, M. Ishihara, T. Ichihara, M. Fukuda, T. Kubo, Y. Gono, A. C. Mueller, R. Anne, D. Bazin, D. Guillemaud-Mueller, R. Bimbot, W. D. Schmidt-Ott, and J. Kasagi, Observation of spin-aligned secondary fragment beams of B^{14}, *Phys. Rev. C* 43(2), 456 (1991)

95. D. Borremans, J. M. Daugas, S. Teughels, D. L. Balabanski, N. Coulier, F. de Oliveira Santos, G. Georgiev, M. Hass, M. Lewitowicz, I. Matea, Y. E. Penionzhkevich, W. D. Schmidt-Ott, Y. E. Sobolev, M. Stanoiu, K. Vyvey, and G. Neyens, Spin polarization of ^{27}Na and ^{31}Al in intermediate energy projectile fragmentation of ^{36}S, *Phys. Rev. C* 66(5), 054601 (2002)

96. K. Turzó, P. Himpe, D. L. Balabanski, G. Bélier, D. Borremans, J. M. Daugas, G. Georgiev, F. O. Santos, S. Mallion, I. Matea, G. Neyens, Y. E. Penionzhkevich, C. Stodel, N. Vermeulen, and D. Yordanov, Spin polarization of Al^{34} fragments produced by nucleon pickup at intermediate energies, *Phys. Rev. C* 73(4), 044313 (2006)

97. Y. Ichikawa, H. Ueno, Y. Ishii, T. Furukawa, A. Yoshimi, D. Kameda, H. Watanabe, N. Aoi, K. Asahi, D. L. Balabanski, R. Chevrier, J. M. Daugas, N. Fukuda, G. Georgiev, H. Hayashi, H. Iijima, N. Inabe, T. Inoue, M. Ishihara, T. Kubo, T. Nanao, T. Ohnishi, K. Suzuki, M. Tsuchiya, H. Takeda, and M. M. Rajabali, Production of spin-controlled rare isotope beams, *Nat. Phys.* 8(12), 918 (2012)

98. N. H. Buttimore, E. Gotsman, and E. Leader, Spin-dependent phenomena induced by electromagnetic-hadronic interference at high energies, *Phys. Rev. D* 18(3), 694 (1978)

99. A. Zelenski, G. Atoian, A. Bogdanov, D. Raparia, M. Runtso, and E. Stephenson, Precision, absolute proton polarization measurements at 200 MeV beam energy, *J. Phys.: Conf. Ser.* 295, 012132 (2011)